**Atmospheric
Measurement
Techniques
Discussions**

# SCIAMACHY lunar occultation water vapor measurements: retrieval and validation results

F. Azam[1], K. Bramstedt[1], A. Rozanov[1], K. Weigel[1], H. Bovensmann[1],
G. P. Stiller[2], and J. P. Burrows[1]

[1]Institute of Environmental Physics (IUP), University of Bremen, Bremen, Germany
[2]Institute for Meteorology and Climate Research (IMK), Karlsruhe Institute of Technology (KIT), Karlsruhe, Germany

Correspondence to: F. Azam (faiza@iup.physik.uni-bremen.de)

Title Page

Abstract | Introduction

Conclusions | References

Tables | Figures

|◄ | ►|

◄ | ►

Back | Close

Full Screen / Esc

Printer-friendly Version

Interactive Discussion

## Abstract

SCIAMACHY lunar occultation measurements have been used to derive vertical profiles of stratospheric water vapor for the Southern Hemisphere in the near infrared (NIR) spectral range of 1350–1420 nm. The focus of this study is to present the retrieval methodology including the sensitivity studies and optimizations for the implementation of the radiative transfer model on SCIAMACHY lunar occultation measurements. The study also includes the validation of the data product with the collocated measurements from two satellite occultation instruments and two instruments measuring in limb geometry. The SCIAMACHY lunar occultation water vapor measurements comparisons with the ACE-FTS instrument have shown an agreement of 5 % on the average that is well within the reported biases of ACE in the stratosphere. The comparisons with HALOE have also shown good results where the agreement between the instruments is within 5 %. The validations of the lunar occultation water vapor measurements with MLS instrument are exceptionally good varying between 1.5 to around 4 %. The validations with MIPAS are in the range of 10 %. A validated dataset of water vapor vertical distributions from SCIAMACHY lunar occultation measurements is expected to facilitate the understanding of physical and chemical processes in the southern mid-latitudes and the dynamical processes related to polar vortex.

## 1 Introduction

SCIAMACHY (SCanning Imaging Absorption spectroMeter for Atmospheric CHartographY) (Burrows et al., 1995) is a moderate resolution 8-channel grating spectrometer on-board Envisat, launched in 2002. The instrument measures solar irradiances and the earthshine radiances from the UV to the NIR (240 nm–2380 nm) spectral region in nadir, limb and solar/lunar occultation geometry. SCIAMACHY is dedicated to improve our knowledge in atmospheric composition and global atmospheric change (Bovensmann et al., 1999). Since the launch of its host satellite, the instrument is providing

F. Azam et al.

total columns as well as vertical profiles of atmospheric parameters relevant to ozone chemistry, air pollution and global climate change issues, from the Troposphere up to the Mesosphere (Gottwald and Bovensmann, 2011).

SCIAMACHY lunar occultation measurements have provided valuable datasets of atmospheric species as ozone, nitrate radical and nitrogen dioxide (Amekudzi et al., 2005, 2009), which have been used for physical and chemical interpretations and analysis.

The lunar occultation coverage is over the southern midlatitudes and polar region for the years 2002–2010.

Water vapor is the most abundant and highly variable green house gas in the Earth's atmosphere. Depending on the latitude and altitude, the distribution of water vapor directly affects the physics, chemistry, dynamics and the radiation in the atmosphere (Solomon et al., 2010). Owing to its longer chemical lifetime with respect to the timescale of the stratospheric dynamical processes, water vapor is used as an excellent tracer of atmospheric circulations and waves etc. (Pan et al., 2007). The primary source of water vapor in the lowermost stratosphere is the adiabatic injection across the tropical tropopause. However this has to pass through the cold trap of the temperature minimum at the tropopause region, above this region the oxidation of methane and other hydrocarbons release hydrogen containing free radicals with $H_2O$ being formed by the reaction with OH. Thus very low water vapor amounts are found in the tropical lower stratosphere due to the air ascending through the cold tropical tropopause region with an annual average of around 3.8 ppmv (Dessler and Kim, 1999). In the upper stratosphere, methane oxidation is the dominant local stratospheric water vapor source (Abbas et al., 1996; Michelsen et al., 2000) and the relationship between stratospheric methane and water vapor has been demonstrated in previous studies (Gurlit et al., 2005). Higher water vapor mixing ratios are observed with increasing altitude reaching around 7 ppmv near the stratopause (Pan et al., 2002). The large scale general circulation across the hemispheres brings the moist air in the polar region where it descends inside the polar vortex. In the polar stratosphere, the water vapor amounts

remain high with the exception of the dehydration events in the polar lower stratosphere due to the formation of polar stratospheric clouds (PSCs). Inside the polar vortex, the water vapor amounts directly influence the ozone depletion by controlling the formation temperatures and the size of the polar stratospheric clouds (Kirk-Davidoff et al., 1999; Kirk-Davidoff and Lamarque, 2008), and the polar vortex temperatures.

SCIAMACHY's measurements in the occultation mode have high accuracy since they are self calibrating. This feature also makes them well suited for the trend analysis.The measurements give localized coverage where the vertical profiles of stratospheric constituents are retrieved with a vertical resolution of 3–4 km.

## 2  SCIAMACHY lunar occultation

SCIAMACHY lunar occultation measurements are carried out over the southern high latitudes between 59° S–89° S during local night time. The latitudinal constraint is due to the sun synchronous orbit of Envisat and the placement of the instrument on the satellite. The properties of moonrise in SCIAMACHY's field of view (FOV) are determined by the orientation of lunar orbital plane with respect to Envisat's orbital plane and the ecliptic. Each measurement starts when the moon rises above a tangent height altitude of around 17.2 km. Below this altitude, the apparent angular rate of the rising true moon is considerably higher than that of the rising refracted images. The moonrise is observed when the phase is >0.5 in the instrument's FOV with solar zenith angle (SZA) >94°. The measurements end shortly after the full moon. The scanner follows the predicted movement of the moon for 16 s, then the moon follower device (MFD) takes over and adjusts the scanner to the brightest point of the moon. The switch is at an altitude of about 65 km. Above 100 km, the measurements are performed for calibration purposes and to calculate transmission.

In the southern polar region, the polar night lasts from April till September. The winter season spans from June to September. The months of July, August and September endure the coldest temperatures. During this period, the heterogeneous chemistry

Title Page

Abstract | Introduction

Conclusions | References

Tables | Figures

◀ | ▶|

◀ | ▶

Back | Close

Full Screen / Esc

Printer-friendly Version

Interactive Discussion

on the surface of PSCs kicks off the formation of the ozone hole. As originally proposed, SCIAMACHY comprised two instruments for limb and nadir. As a result of cost reduction imposed by the space agencies, the instrument aboard Envisat in its sun synchronous orbit comprised one instrument undertaking solar occultation in the

5 Northern Hemisphere, alternate but matched limb and nadir during an orbit and lunar occultation in the Southern Hemisphere. On the average, the yearly SCIAMACHY lunar occultation measurements extend from November to June owing to the limitations described above. Occasionally there are few measurements in October. This measurement pattern implies that the atmospheric species participating in the heterogeneous

10 chemistry and chemical processes at high latitudes cannot be obeserved between July and September. In the southern polar stratosphere, the formation of vortex begins to spin up in March and as a result of momentum transport to high latitudes is lost typically in November or December. The quantitative analysis of water vapor distributions and variability in the polar stratosphere provides a perspective into the evolution and the

15 break down of the polar vortex. The strong relationship between water vapor and the upper atmospheric dynamics has been established in various studies (Russell et al., 1993a; Lahoz et al., 1993, 1996). The retrieval of stratospheric water vapor from SCIAMACHY lunar occultation measurements yields some unique insight into the dynamics of the stratosphere and provides the motivation behind the study.

## 20  3  Solar zenith angle and the moon phase distribution for the lunar occultaion measurements

The geographical distribution of SCIAMACHY lunar occultation measurements is sparse as can be seen in the example in Fig. 1 which shows the tangent points for the year 2010. Figure 2 shows the latitudinal distribution time series for the years

25 2003–2010. As clearly seen, there is a large latitudinal variation within a month and over a year. This is due to the fact that the sub satellite point's latitude changes considerably at the moonrise within a month. This feature makes the measurements suitable

Full Screen / Esc

Printer-friendly Version

Interactive Discussion

for studying the southern polar atmosphere at various latitudes during a year. On the average, each year the measurements span is ~59° S–89° S from January till June. In November and December, the measurements are limited to 60° S–70° S.

The yearly time series of solar zenith angle (SZA) and moon phase for SCIAMACHY lunar occultation measurements are shown in Figs. 3 and 4, respectively. The SZA variation for each year is between 94° and 115° with the highest values observed around April. The observed moon phase values vary around 0.5–0.99. The assignment of phase follows as for the half moon, the phase is 0.5 and so on. The smaller the SZA value, the higher is the influence of the scattered light from the sun, whereas for moon phase, the higher values signify a strong signal. The quality of the SCIAMACHY lunar occultation spectral signal is essentially determined by the values of the SZA and the moon phase. The quality criteria thus implied was the selection of measurements with moon phase $\geq$ 0.75 and SZA $\geq$ 96°. On the average, the usable SCIAMACHY lunar occultation measurements are 6 days a month and 6–8 months in a year.

## 4 Retrieval theory

This section explains the retrieval method implied on the SCIAMACHY lunar occultation measurements. The scheme is explained in depth in Amekudzi (2005) and the references therein and will be described here in brief with emphasis on the theory that is essential to understand the contents of Sect. 5. The basic equation to be solved is a non-linear, ill-posed inverse problem (Rodgers, 2000)

$$\boldsymbol{y} = F(\boldsymbol{x}, \boldsymbol{b}) + \boldsymbol{\varepsilon} \tag{1}$$

relating the measurement vector $\boldsymbol{y}$ i.e. the measured lunar spectrum, by a forward model $F$. The state vector $\boldsymbol{x}$ represents the water vapor vertical profile to be estimated. The forward model $F$ accounts for the physics of the measurement including the instrument characterization. The vector $\boldsymbol{b}$ includes the model parameters as line strength, pressure broadening, temperature etc. The symbol $\boldsymbol{\varepsilon}$ represents errors of all

kind. Equation (1) is linearized with respect to a reference state signifying the first estimate of the true atmospheric state, termed as the a priori $x_a$. The a priori is introduced by a climatology. The linearization is performed by using the Taylor series expansion and neglecting its higher terms

$$y = F(x_a) + \frac{\partial F(x)}{\partial x}|_{x_a}(x - x_a) + \varepsilon \qquad (2)$$

where the differential on the right handside is the weighting function matrix taking into account the sensitivity of the measurement to the true profile. It is denoted by $\mathbf{K}$, $\mathbf{K} \approx \partial y/\partial x$. Thus

$$\hat{y} = y - y_a = \mathbf{K}\hat{x} + \varepsilon = \mathbf{K}(x - x_a) + \varepsilon \qquad (3)$$

relates the measurement state vector $\hat{y}$ and the model state vector $\hat{x}$, $y_a$ is the simulated a priori spectra. The retrieval solution is obtained by applying the optimal estimation and using the Newton iterative scheme as described in Rodgers (2000), which, for an $(i + 1)$-th step, results in

$$x_{i+1} = x_a + (\mathbf{K}_i^T \mathbf{S}_y^{-1} \mathbf{K}_i + \mathbf{S}_a^{-1})^{-1} \mathbf{K}_i^T \mathbf{S}_y^{-1}$$
$$(y - y_i + \mathbf{K}_i(x_i - x_a)) \qquad (4)$$

with $\mathbf{S}_a$, the constraint matrix for the state vector called a priori covariance matrix reflecting uncertainties of the a priori height profiles, and $\mathbf{S}_y$ as the measurement error covariance matrix representing the measurement noise for every measurement and wavelength. In Eq. (4)

$$\mathbf{D}_i = (\mathbf{K}_i^T \mathbf{S}_y^{-1} \mathbf{K}_i + \mathbf{S}_a^{-1})^{-1} \mathbf{K}_i^T \mathbf{S}_y^{-1} \qquad (5)$$

is the contribution function representing the sensitivity of the retrieval to the measurement implying $\mathbf{D} \approx \partial \hat{x}/\partial y$. The convergence to terminate the iterations is achieved when the measurement residuals $y_i - y$ are sufficiently small or the retrieved profile does not change anymore during the iterations.

Inverse problems in general are sensitive to small perturbations that may introduce unrealistic features. In our study, the inversion was stabilized by using an optimization approach which suppresses the additive noise. A regularization term called the Tikhonov regularization (Tikhonov, 1963; Tikhonov and Y., 1997) was introduced in the retrieval solution by extending the inverse of the a priori covariance matrix by Tikhonov matrix as

$$\mathbf{S}_a^{-1} \longrightarrow \mathbf{S}_a^{-1} + \mathbf{S}_t^T \mathbf{S}_t \tag{6}$$

This constrains the smoothness of the retrieved profile $\hat{x}$ contributing to the desired state of the retrieved atmospheric parameter. In Eq. (6), $\mathbf{S}_t$ is the first order derivative matrix weighted by an appropriate parameter termed Tikhonov parameter. An appropriate value of Tikhonov parameter has to be selected, as will be shown in Sect. 5.4.4, minimizing the loss of information.

The retrieval solution covariance matrix (smoothing error and retrieval noise) corresponding to Eq. (4), is given by

$$\mathbf{S} = (\mathbf{K}_i^T \mathbf{S}_y^{-1} \mathbf{K}_i + \mathbf{S}_a^{-1})^{-1} \tag{7}$$

The diagonal elements of $\mathbf{S}$ are the covariances of the retrieved water vapor profiles and are the indicators of the theoretical precision of the retrieval.

# 5 Water vapor retrieval

## 5.1 Data

The data used for the the retrieval was the SCIAMACHY lunar occultation level 1b (l1b) data provided by ESA. In our study the versions 6.03 and 7.0 were used to derive the vertical profiles of stratospheric water vapor from $\sim$17–50 km in the NIR spectral region.

## 5.2 Wavelength window

The wavelength window available in the NIR region for the retrieval of SCIAMACHY lunar occultation water vapor profiles was 1350–1450 nm in channel 6 of the spectrometer. Figure 5 shows a spectral fit plot for this window. The green line is the modelled differential optical depth and the red line represents the measured differential spectrum of water vapor. The calculation of these spectra will be described later in this section. The spectral window 1350–1450 nm contains a strong absorption by $CO_2$ around 1430 nm. To obviate any complexity arising from the ESFT radiative transfer method (see Sect. 5.4) in handling two absorbers in the same window, the wavelength section 1350–1420 nm was selected as the extraction and retrieval wavelength window. A good fit was observed for 1350–1420 nm. Figure 6 shows the residual plot associated to Fig. 5, signifying the difference between the measured and the simulated differential spectra. As can be seen, the residuals are of the order of 0.5 % which is within the signal to noise ratio.

## 5.3 Lunar spectrum extraction

The raw lunar radiance spectra are calibrated for offsets as nonlinearlity, straylight and dark current correction. In addition the spectral calibration is performed. Proceeding these corrections and calibration, the lunar spectrum $I^l(h_i, \lambda)$ was extracted for 13 tangent heights $h_i$, between 17–50 km, selecting the 14th at 120 km which was the reference spectrum $I^{ref}(h_i, \lambda)$. The NIR detectors of SCIAMACHY contain some bad pixels. Two bad pixels were identified in the wavelength region 1350–1420 nm and excluded.

## 5.4 Retrieval methodology, sensitivity studies and optimizations

A robust and efficient inversion scheme and retrieval algorithm, SCIATRAN, is implemented on SCIAMACHY measurements for the retrieval of atmospheric parameters from the ultraviolet to near infrared region. This algorithm was developed at Institute of

**SCIAMACHY lunar occultation water vapor measurements**

F. Azam et al.

Title Page

| Abstract | Introduction |
| Conclusions | References |
| Tables | Figures |

◄◄  ►►

◄  ►

Back  Close

Full Screen / Esc

Printer-friendly Version

Interactive Discussion

Environmental Physics/Remote Sensing, University of Bremen (Rozanov, 2001), as an extension of UV-Visible GOMETRAN radiative transfer model (Rozanov et al., 1997). The vertical profiles of water vapor from SCIAMACHY lunar occultation observations were retrieved using SCIATRAN version 3.0. In the framework of an optimal estima-

5  tion approach, SCIATRAN is applied as a forward model i.e. a radiative transfer model (RTM) and a retrieval code i.e. the inverse part which fits the results from the former to the real measurements. The spectral absorption line features were treated by using the exponential sum fitting of transmissions coefficients method, ESFT, (Sect. 5.4.3) employing correlated-$k$ distribution instead of the line by line (LBL) treatment of the line

10  absorbers. The retrieval methodology for the ESFT approach is illustrated in Fig. 7.

## 5.4.1  Forward model/radiative transfer part

The forward model or the radiative transfer part takes input parameters as initial water vapor profile i.e. the a priori, viewing angles, pressure and temperature distributions, cross sections and instrument slit function. For the current retrieval, the initial guess

15  and a prior along with the temperature and pressure were taken from the US Standard Atmosphere climatology (1976). The ESFT database is calculated, at the given temperature and pressure, from the HITRAN database (Rothman et al., 2009) that contain individual absorption lines. The SCIATRAN forward model performs two functions, namely, simulating the transport of radiation through the atmosphere and computing

20  the weighting functions.

For the construction of the forward model, the differential optical depths were considered rather than the radiances themselves (Rozanov et al., 2000, 2005). This took into account the logarithm of the measured radiances. The logarithms increase the linearity of the inverse method applied thereby reducing the linearization errors (Hoogen

25  et al., 1999; Rozanov et al., 2011). A fitted third order (low order) polynomial $P(3)$ in wavelength $\lambda$ was then subtracted to reduce the effect of the broad band features. This whole approach was applied to the measured radiance at each tangent height $j$, the

radiance at the reference tangent height (note: both are represented by one Eq. 8) and the simulated radiances.

$$\widetilde{I}_j(\lambda) = \ln\left[I_j(\lambda)\right] - P(3)$$

$$= \ln\left[I_j(\lambda)\right] - \sum_{i=0}^{N=3} c_j^k \lambda^i \tag{8}$$

5    The tangent height and polynomial indexes are represented by $j$ an $i$, respectively and $c$ is the coefficient of the polynomial. The superscript $k$ is the retrieval parameter index. Spectra of differential optical depth were used. To obtain them, the measured transmission spectra were divided by a reference spectrum (at 120 km altitude). This implies, numerically

10    $$y_j = \frac{\ln(I^l(\lambda))}{\ln(I^{ref}(\lambda))} \tag{9}$$

The simulated transmission differential spectra defining the forward model were obtained in a very similar manner.

The variation or the response of the measured radiation due to the change in the vertical profile of the atmospheric parameter $\alpha_i$, here water vapor, at a spectral point

15    $\lambda_i$, is mathematically termed the weighting function at the altitude $h_i$ under consideration. The weighting functions are elements of the matrix **K**, from Eq. (3), and hence are the derivatives of the measured intensity $I$ with respect to the relative trace gas concentration $\alpha_i$

$$W_j(h_i, \lambda) = \frac{\partial I(\lambda)}{\partial \alpha_i} \alpha_i \tag{10}$$

20    These are the relative weighting functions and are also transformed to the differential form for the same reason described above. Thus

$$\hat{W} = \frac{1}{I_j^s(\lambda)} W_j^k - \frac{1}{I_{ref}^s(\lambda)} W_{ref}^k - \sum_{i=0}^{N=3} c_j^i \lambda^i \tag{11}$$

Here $I^s$ are the simulated differential spectra. For the lunar occultation, the effect of errors resulting from wavelength calibration and Doppler shift etc. were reduced by applying a shift and squeeze correction. Such correction of individual spectra improves wavelength misalignments between weighting functions, radiances and reference spectra. In our study, the correction was carried out by implying non linear least square method, with iterations, thereby reducing the following quadratic form for each tangent height.

$$\|\widetilde{I}_j^s(\lambda) + \sum_k \hat{W}_j^k(\lambda)\frac{\Delta\alpha^k}{\alpha^k} - \widetilde{I}_j^l(\lambda) + \widetilde{I}^{ref}(\lambda) - b_{shi}\frac{\delta\widetilde{I}_j^s(\lambda)}{\delta\lambda}$$
$$- b_{sq}\frac{\delta\widetilde{I}_j^s(\lambda)}{\delta\lambda}\lambda - \frac{\delta\widetilde{I}^{ref}(\lambda)}{\delta\lambda}\|^2 \to m \tag{12}$$

In the above equation, $W_j^k(\lambda)$ are the vertically integrated weighting functions with scaling of the vertical profile as $\Delta\alpha^k/\alpha^k$ which is constant for each layer. $b_{sh}$ and $b_{sq}$ are the shift and squeeze parameters at a given tangent altitude. This pre-processing step by SCIATRAN improved the residuals specially for the lower stratospheric tangent heights.

## 5.4.2 Inversion/retrieval part

The theoretical aspects of the retrieval technique are explained in Sect. 4 which involves solving the inverse problem by implementation of the optimal estimation to get the desired parameter and applying Newton iterative scheme for the convergence of the solution. The retrieval procedure is sketched in Fig. 7. As shown in the figure, the retrieval can be divided into two parts. In the first part, the difference between the measured and the simulated spectrum is calculated. The second part takes the parameters as a priori, signal to noise ratio and Tikhonov regularization and applies optimal estimation on the result from the former composing the vertical profile of water vapor. The optimizations related to signal to noise ratio and Tikhonov regularization parameter will be discussed in the next section. The profile obtained is fed back to the forward model

section where the simulation and computations are done again. A number of iterations are carried out till the conditions described in Sect. 4 are achieved. The final retrieval profile, approximating the true atmospheric state was obtained in this manner.

### 5.4.3 The line absorber treatment

As mentioned before in Sect. 5.4, the line absorbers treatment is carried out using ESFT approximation (Wiscombe and Evans, 1977) employing correlated-$k$ approach and not the LBL method. The LBL radiative transfer is a monochromatic method involving computations of radiance for each frequency in a selected wavelength window. The radiances are then integrated over this region. It should be noted that LBL method is assumed to be a true representative of the reality compared to the ESFT approximation. LBL computation has to be carried out with sufficiently fine grid (0.001 nm/line or less) to accurately reproduce the absorption coefficient spectrum and to perform correct radiative transfer calculations. The LBL calculations thus require substantial computing time. Therefore ESFT is preferred over LBL. When LBL is used in SCIATRAN, the line parameters as line intensities, line locations etc. are taken from HITRAN 2008.

By definition, ESFT is a method of fitting the transmission functions by exponential sums to calculate the spectrally integrated radiative fluxes. In the correlated-$k$ distribution method, the spectrum is binned according to the strength of absorption and radiative transfer equation is integrated for all atmospheric layers under consideration. The binning is based on the observations that the maxima and minima of absorptions in different layers coincide spectrally. The implementation of this method in SCIATRAN is discussed in detail in Buchwitz et al. (2000). ESFT is a fast retrieval method and its usage in SCIATRAN involves the calculation of the ESFT coefficients using HITRAN 2008 database. Mathematically, in general the absorption coefficients for simple LBL computation are given as

$$k_\lambda(p,t) = \sum_i S_i(t) f_i(\lambda,p,t) \qquad (13)$$

Title Page

Abstract | Introduction

Conclusions | References

Tables | Figures

◀ | ▶

◀ | ▶

Back | Close

Full Screen / Esc

Printer-friendly Version

Interactive Discussion

where $p$ and $t$ are pressure and temperature, respectively. $S_i$ is the line intensity for the ith absorption line and $f_i(\lambda, p, t)$ stands for the line shape factor. The spectrally mean transmittance over the spectral interval $\Delta\lambda$ can be approximated as

$$T_{\Delta\lambda}(m) = \int_{\Delta\lambda} \left[ exp(-k_\lambda m) \right] \frac{d\lambda}{\Delta\lambda} \tag{14}$$

5  here $m$ is the absorber amount per unit area. In any wavelength window, the same values of $k(p, t)$ occur frequently. This means that the computational efficiency can be improved by replacing the integration over $\lambda$ in Eq. (14) by the probability distribution function of absorption coefficient, $h(k)$, and further by their cumulative probability distribution $g(k)$ (Fu and Liou, 1992; Li and Barker, 2004)

$$
\begin{aligned}
10 \quad T_{\Delta\lambda}(m) &= \int_0^\infty \left[ \exp(-k_\lambda m) \right] h(k) d(k) \\
&= \int_0^1 \left[ \exp(-k_g m) \right] dg
\end{aligned}
\tag{15}
$$

$h(k)dk$ is the fraction of $\Delta\lambda$ where the absorption coefficient value is between $k$ and $k + dk$ and by definition $g(k)$ is monotonically and smoothly increasing function in $k$ space.

$$15 \quad g(k) = \int_0^1 h(k) dk \tag{16}$$

At different temperature/pressure in the atmosphere, the cumulative probability distribution space of the absorption coefficients are correlated (Kratz et al., 1998). For such a correlation of absorption coefficients, an optimum number of $k$ values can be selected to further reduce the computing time. The optimization method of choice in this
20  case is the ESFT approximation. In the ESFT approach, the spectral mean transmission is approximated by a quadrature of absorption coefficients $k_i(p, t)$ with weights $w_i$ and nodes $g_i$.

$$T_{\Delta\lambda}(m) = \sum_{i=0}^{n} w_i \left[ \exp(-k_\lambda m) \right] \qquad (17)$$

$$\text{where} \quad k_i = k(g_i) \quad \text{and} \quad \sum_i w_i = 1 \qquad (18)$$

HITRAN 2008 database for ESFT implementation contains the spectral ranges, their corresponding line absorbers, and as explained above, the number of coefficients calculated at a number of temperature and pressure grid points for each case. As will be seen in the next section, in our study, different grids for the water vapor window 1240–1560 nm created at IUP were tested for the retrieval.

### 5.4.4 Sensitivity studies and optimizations

To account for the finite resolution of the instrument, the simulated radiance has to be convolved with an appropriate instrument slit function. In ESFT technique, the internal wavelength grid for convolution is read from ESFT database for RTM calculations.

The signal to noise ratio was estimated from the fit residuals at the preprocessing step.

The smoothness of the retrieval profile was constrained by Tikhonov regularization (Eq. 6). Figure 8 shows the number density profiles for different Tikhonov parameters and Fig. 9 shows the theoretical errors arising from these selected numbers. It can be seen that the higher values of the smoothness parameter cause loss of information (Fig. 8) keeping the errors low while the lower values are unable to remove the oscillations and introduce errors (Fig. 8). An appropriate Tikhonov value, 3.5, was selected preventing loss of measurement information.

As mentioned before, convolution is applied to the simulated spectrum according to the instrument slit function. A Gaussian type slit function was used. The parameter defining the width of the slit function is the full width at half maximum (FWHM). Since the knowledge about SCIAMACHY slit function is limited, the value for the FWHM was

optimized with respect to the fit residuals. The value of FWHM giving minimum retrieval residuals was selected. The residuals were found to be minimum at the FWHM of 1.30 nm.

Following the sensitivity studies, the quality of the retrieval performed using ESFT technique was first verified by comparison with the profiles retrieved from the LBL. As mentioned earlier, compared to the ESFT approximation, theoretically LBL is considered to be the true representative of reality. Owing to the computational cost, the lunar occultation spectra were retrieved by using LBL method for only one randomly selected year, 2008. For the same year, the ESFT retrieval was performed using grids with different pressure ($P$), temperature ($T$) and coefficients ($C$) as shown in Table 1. The objective was to make the ESFT retrieved profiles agree with the line by line retrieval. Figure 10 illustrates the results of the comparisons as LBL-ESFT relative difference plots for the profiles of 2008 retrieved on different ESFT grids. As can be observed in the figure, changing the number of pressure and temperature grid points has less impact on the results. Increasing the number of coefficients (from 10 to 15) is seen to bring the two techniques in good agreement, specifically as clear in the figure, the LBL-ESFT difference is reduced from 15–20 % to around 3.5 % in the middle stratosphere. It should be mentioned here that increasing the number of coefficients increases the computational time. Conclusively, the grid with 32 pressures, 22 temperatures and 15 coefficients was found to give the closest match between the ESFT and LBL retrieval where the overall LBL-ESFT agreement is within 1 to around 3.5 % from 17–50 km.

# 6 Averaging kernels

Equation (5) describes the gain matrix which signifies the sensitivity of the retrieved profile to the measurement. The sensitivity of the profile to the true profile is given by the averaging kernel matrix $\mathbf{A}$, where $\mathbf{A} = \mathbf{DK}$, $\mathbf{A} \approx \partial \hat{x} / \partial x$. Therefore

$$\mathbf{A} = (\mathbf{K}_i^T \mathbf{S}_y^{-1} \mathbf{K}_i + \mathbf{S}_a^{-1})^{-1} \mathbf{K}_i^T \mathbf{S}_y^{-1} \mathbf{K} \tag{19}$$

Full Screen / Esc

Along with sensitivity of the retrieval, the averaging kernel matrix characterizes its vertical resolution. At a given altitude, the averaging kernels are peaked functions. The vertical resolution is given by their width where a measure of the width at a given height can be (FWHM) see Sect. 5.4.4. The sum of all elements (rows) of the averaging kernel matrix is often termed the measurement response in the literature (Rodgers, 2000). When it is close to unity, the observing system is sensitive to the true profile. Values less than unity signify the influence of the a priori on the retrieval.

The averaging kernels for SCIAMACHY lunar occultation water vapour retrieval employing ESFT approach in the RTM are shown in Fig. 11. These were based on the 1 km grid SCIATRAN used for radiative transfer calculations. The averaging kernels of several altitudes have peaks at the same level due to the difference between SCIA-MACHY's vertical sampling (3.3 km) and the retrieval grid (1 km). In general, the averaging kernels below 47 km have sharp peaks indicating high sensitivity of the retrieval for this range. The response function plotted in the right panel of Fig. 11 shows that between 17 and 47 km, the retrieval profile is determined only by the measurement (value $\approx$ 1). Above 47 km there is some contribution from the a priori (value < 1).

# 7 Water vapor profiles

Figure 12 gives an example of the retrieved SCIAMACHY lunar occultation water vapor number density profile for the southern polar stratosphere from 17–50 km. The profile is for 10 January 2009. The correlative ACE-FTS, MLS and MIPAS are also plotted in the figure. The water vapor volume mixing ratios (vmr) from these four instruments were converted to number densities using the temperatures and pressures measured by these instruments. The number densities were then interpolated to the retrieval altitude grid of SCAIAMACHY measurements for comparison.

## 8   Comparisons/validations

To assess the quality of the SCIAMACHY lunar occultation water vapor profiles, the validation was performed with collocated measurements from the satellite instruments ACE-FTS and HALOE, which are occultation instruments and MLS and MIPAS, that perform measurements in the limb geometry.  The SCIAMACHY water vapor data showed evidence of PSCs as early as May.  Such PSCs contaminated profiles were filtered out on the basis of the temperature thresholds for the production of all types of PSCs. The formation temperature for the type I PSCs i.e. Nitric Acid Trihydrate (NAT, crystaline) is less than 195 K and the type II PSCs i.e. pure ice, can form at temperatures lower than approximately 188 K (von Savigny et al., 2005; Peter, 1997).  The ECMWF analysis profiles corresponding to the SCIAMACHY water vapor profiles were used as source of temperature information.

For the comparison with SCIAMACHY data, as mentioned before, the water vapor vmr from the four instruments were converted to number densities.  The coincidence search was based on the criteria of selecting all the measurements within the maximum collocation radius of 1000 km and having maximum time difference of 12 h between SCIAMACHY overpass and the correlative measurements from the instruments.

The comparisons are plotted showing the following statistics:

*rmd* The relative mean difference between the SCIAMACHY and other instrument weighted by the average.

*rmd std.* The standard deviation of the ensemble of relative mean differences giving an insight into the variability of the individual comparisons.

*bias std. err.* The rmd can be seen as measurement of the bias of SCIAMACHY to the other instrument.  The standard error of the bias is the standard deviation of the ensemble divided by the square root of the number of coincidences.

As clear in Figs. 13, 14, 15, 16, the standard error of the bias is very small in all cases as the number of coincidences is large. All biases discussed in the following section are significant regarding its standard error.

## 8.1 ACE-FTS

The Atmospheric Chemistry Experiment Fourier Transform Spectrometer (ACE-FTS) onboard Canadian Scientific Satellite SCISAT is performing solar occultation measurements in the infrared since 2004 (Bernath, 2005). The vertical resolution of the instrument is consistent with that of SCIAMACHY lunar occultation which is 3–4 km. The water vapor vmr from ACE-FTS are retrieved from 5 to 90 km (Carleer et al., 2008). For the presented study, ACE-FTS version 2.2 water vapor product was used. The comparison of this version of ACE with various ground based and space borne instruments have shown that ACE-FTS is biased positive (wet bias) in the order of 3–10 % between 15–70 km according to Carleer et al. (2008).

With the collocation criteria described above and for the period of 2004–2009, 302 collocations were found for both sunrise and sunset ACE-FTS events. Figure 13 shows the statistics plotted for the altitude range 17–50 km. The SCIAMACHY-ACE rmd is observed to be within −1.5 % from 17 to 22 km, about −5 % for 23–42 km, around −(6–7) % between 43–47 km and within −10 % for the altitude range 48–50 km. Hence in general the rmd are below −7 %. The rmd std. are within 5 % from 17 to 29 km and increase to 7–10 % from 30 to 50 km. The above mentioned wet bias in ACE-FTS water vapor measurements is also seen by SCIAMACHY lunar occultation measurements. From this evidence, it can be concluded that the SCIAMACHY-ACE agreement is good being well within the reported biases of ACE-FTS.

## 8.2 HALOE

The Halogen Occultation Experiment HALOE was launched on Upper Atmosphere Research Satellite (UARS) in 1991 (Russell et al., 1993b) and the mission ended in 2005.

HALOE used infrared solar occultation to measure the vertical profiles of different climate parameters from 15 to 85 km with a vertical resolution of around 2.3 km. The version-19 of HALOE water vapor profiles was used in our study. The extensive validations of HALOE water vapor measurements have shown that HALOE is biased low (dry bias) by 5 % in the stratosphere (Harries et al., 1996; Kley et al., 2000).

The coincidence search with the criteria employed for the years 2003–2005 resulted in 52 coincidences with HALOE sunrise events and none with sunset. Figure 14 shows the statistics of SCIAMACHY-HALOE comparisons. The rmd are 10 % at 17 km, 6 % at 18 km, about 1 % between 19–24 km, vary around 5 % from 25 to 40 km, within 7.5 % for 41–43 km and reach about 10 % at 50 km. The rmd std. vary between 3.5–4.5 % from 17 to 33 km, 5–6 % at 34–42 km, around 7.5 % for the altitudes 43–48 km and then 10 % to 50 km. Keeping the dry bias in the HALOE measurements in view, the SCIAMACHY-HALOE difference is an indicative of the influence of the HALOE bias in the comparisons.

## 8.3 MLS

The EOS-MLS (Earth Observing System-Microwave Limb Sounder) was launched on NASA's satellite EOS-Aura in 2004. MLS makes atmospheric measurements from 8 to 90 km by observing thermal microwave emissions from the earth's limb (Waters et al., 2006; Schoeberl et al., 2006). In the altitude region of about 18–54 km (100–1.0 hPa), the vertical resolution of MLS is 3.5–4.6 km. MLS water vapour version 2.2 was used for the validation of lunar occultation water vapour profiles because it is an extensively validated MLS water vapor product. For the comparison, the MLS geopotential height was converted to geometric height using the MLS pressure and temperature.

The SCIAMACHY-MLS validation was based on 1321 collocated measurements for the period 2004–2010. The comparison result is shown in Fig. 15 where the rmd vary between (1.5–4) % from 17–34 km with the exceptions at about 22, 24 and 27 km where it is in the range ±(4.5–6) %. The rmd are within −(1–1.5) % for 35–46 km, and within −3 % from 47 to 50 km. The rmd std. range between 6–7.5 % for the whole altitude

of 17–50 km. It should be noted here that in its comparisons with other satellite instruments including ACE-FTS, HALOE and MIPAS, the MLS water vapor version 2.2 is noted (Lambert et al., 2007) to exhibit sharp differences or kink around 26.1 hPa–31.6 hPa which is the region within a few kilometres from 25 km. This problem is corrected in MLS version 3.3 processing algorithm. The SCIAMACHY-MLS exceptional agreement, apart from the above mentioned difference arising due to MLS, validates the good quality of our retrieval and the lunar occultation water vapor dataset. Moreover, MLS, as measuring in microwave, is far less sensitive to clouds and aerosol (Livesey et al., 2006; Waters et al., 2006) that may contaminate any other shorter wavelength region. The SCIAMACHY-MLS excellent agreement shows that the lunar occultation water vapor measurements used for the validations are void of any contaminations.

## 8.4   MIPAS

MIPAS (Michelson Interferometer for Passive Atmospheric Sounding) is one of the ten instruments including SCIAMACHY onboard Envisat satellite. The instrument is a mid-infrared limb emission Fourier transform spectrometer measuring atmospheric profiles of temperature and various constituents of atmosphere from 6–68 km (Fischer et al., 2008). The vertical resolution of MIPAS varies from around 2.3 km (at 20 km) to about 6.9 km (at 50 km) (von Clarmann et al., 2009). The water vapor data version V40_H2O_203 retrieved from the IMK-IAA data processor was used in the presented comparison. The comparison of this MIPAS water vapor data is performed with various ground based and satellite instruments in the framework of MOHAVE-2009 campaign which took place at a location of 34.4° N, 117° W on 12–26 October 2009. The details and results of this study are reported in Stiller et al. (2011). It must be noted that the aim of this campaign was to compare the MIPAS data primarily with highly accurate and precise ground based and balloon borne measurements. The MIPAS water vapor profiles are reported to be within ±10 % of the profiles with the correlative measurements

**SCIAMACHY lunar occultation water vapor measurements**

F. Azam et al.

Title Page

| Abstract | Introduction |
| Conclusions | References |
| Tables | Figures |

|◄ | ►|

◄ | ►

Back | Close

Full Screen / Esc

Printer-friendly Version

Interactive Discussion

of most of the instruments which is within the bias regime among ground based instruments comparisons.

With the collocation criteria as employed in our study, and for the period of 2005–2010, 489 correlative incidences were found between SCIAMACHY and MIPAS. Figure 16 shows the SCIAMACHY-MIPAS comparison results. The rmd is within $-(1-4.5)\,\%$ from 17 to 22 km, around $-7.5\,\%$ at 23–26 km, reach $-9\,\%$ for the altitude range 27 km to about 38 km, $-(2.5-4.5)\,\%$ between 39 to 44 km and within $-1.5\,\%$ for 45–50 km. The rmd std. are about 7.5 % and gradually reach 10 % at 50 km. The SCIAMACHY-MIPAS agreement is within the above mentioned MIPAS bias.

## 9   Conclusions and outlook

The SCIAMACHY lunar occultation measurements have been used to derive the water vapor profiles for the southern hemispheric high latitudes. The retrieval optimizations and sensitivity studies are stepwise presented here. We have demonstrated that for the ESFT method employed with correlated-$k$ approach, the number of coefficients is crucial for the quality of the retrieval. A very close agreement between ESFT and LBL can be achieved by increasing the number of coefficients and thus preventing any systematic biases in the resulting ESFT profiles. The SCIAMACHY lunar occultation water vapor measurements comparisons with the collocated ACE-FTS, HALOE, MLS and MIPAS measurements have shown the agreements that are well within the reported and published uncertainties/biases of these instruments. Based on the presented validations we can conclude that with SCIAMACHY lunar occultation we have retrieved a very good quality water vapor product (version 1.0).

From the SCIAMACHY lunar occultation, the retrieval of water vapor is succesfully carried out in the NIR implying that other gases with spectral signatures in the same region as methane, $CH_4$ and carbon dioxide, $CO_2$ can also be retrieved from lunar occultation.

For the southern hemispheric stratosphere, the in situ water vapor measurements are still in their initial stages and are not available for validation purposes. The SCIA-MACHY lunar occultation water vapor dataset is unique for the southern hemispheric stratospheric region. The product can be used in the models investigating polar vortex dynamics. With these measurements, the formation of PSCs can be studied as early as May–June for the southern region. The dataset is expected to give good results in interpretations and analyses studies. The lunar occultation water vapor measurements will add as a southern hemispheric coverage to the SCIAMACHY long-term global water vapor time series.

**References**

NASA: US Standard Atmosphere Supplements, US Government Printing Office, Washington DC, 1976. 1038

Abbas, M. M., Gunson, M. R., Newchurch, M. J., Michelsen, H. A., Salawitch, R. J., Allen, M. L., Abrams, M. C., Chang, A. Y., Goldman, A., Irion, F. W., Moyer, E. J., Nagaraju, R., Rinsland, C. P., Stiller, G. P., and Zander, R.: The hydrogen budget of the stratosphere inferred from ATMOS measurements of $H_2O$ and $CH_4$, Geophys. Res. Lett., 23, 2405–2408, doi:10.1029/96GL01320, 1996. 1031

Amekudzi, L., Bracher, A., Meyer, J., Rozanov, A., Bovensmann, H., and Burrows, J. P.: Lunar occultation with SCIAMACHY, First retrieval results, Adv. Space Res., 5, 906–914, 2005. 1031

Amekudzi, L. K.: Stratospheric $O_3$, $NO_2$, and $NO_3$ number density profiles from SCIAMACHY lunar occultation spectroscopic measurements: Retrieval, validation and interpretation, Ph.D. thesis, Universität Bremen, 2005. 1034

Amekudzi, L. K., Bramstedt, K., Rozanov, A., Bovensmann, H., and Burrows, J. P.: Retrievals of trace gas concentratioins from lunar occultation measurements with SCIAMACHY on EN-VISAT, in: New Horizon in occultation Research: Studies in Atmosphere and Climate, 2009. 1031

Bernath, P. F.: Atmospheric Chemistry Experiment (ACE): Mission overview, Geophys. Res. Lett., 32, 1–5, doi:10.1029/2005GL022386, 2005. 1047

Bovensmann, H., Burrows, J. P., Buchwitz, M., Frerick, J., Noel, S., Rozanov, V. V., Chance, K. V., and Goede, A. P. H.: SCIAMACHY: Mission Objectives and Measurement Modes, J. Atmos. Sci., 56, 127–150, doi:10.1175/1520-0469(1999)056<0127:SMOAMM>2.0.CO;2, 1999. 1030

Buchwitz, M., Rozanov, V. V., and Burrows, J. P.: A correlated-k distribution scheme for overlapping gases suitable for retrieval of atmospheric constituents from moderate resolution radiance measurements in the visible/near-infrared spectral region, J. Geophys. Res., 105, 5247–15261, doi:10.1029/2000JD900171, 2000. 1041

Burrows, J. P., Holzle, E., Goede, A. P. H., Visser, H., and Fricke, W.: SCIAMACHY – Scanning Imaging Absorption Spectrometer for Atmospheric Chartography, Acta Astronaut, 35, 445–451, 1995. 1030

Carleer, M. R., Boone, C. D., Walker, K. A., Bernath, P. F., Strong, K., Sica, R. J., Randall, C. E., Vömel, H., Kar, J., Höpfner, M., Milz, M., von Clarmann, T., Kivi, R., Valverde-Canossa, J., Sioris, C. E., Izawa, M. R. M., Dupuy, E., McElroy, C. T., Drummond, J. R., Nowlan, C. R., Zou, J., Nichitiu, F., Lossow, S., Urban, J., Murtagh, D., and Dufour, D. G.: Validation of water vapour profiles from the Atmospheric Chemistry Experiment (ACE), Atmos. Chem. Phys. Discuss., 8, 4499–4559, doi:10.5194/acpd-8-4499-2008, 2008. 1047

Dessler, A. and Kim, H.: Determination of the amount of water vapor entering the stratosphere based on Halogen Occultation Experiment (HALOE) data, J. Geophys. Res., 104, 30605–30607, 1999). 1031

Fischer, H., Birk, M., Blom, C., Carli, B., Carlotti, M., von Clarmann, T., Delbouille, L., Dudhia, A., Ehhalt, D., Endemann, M., Flaud, J. M., Gessner, R., Kleinert, A., Koopman, R., Langen, J., López-Puertas, M., Mosner, P., Nett, H., Oelhaf, H., Perron, G., Remedios, J., Ridolfi, M., Stiller, G., and Zander, R.: MIPAS: an instrument for atmospheric and climate research, Atmos. Chem. Phys., 8, 2151–2188, doi:10.5194/acp-8-2151-2008, 2008. 1049

Fu, Q. and Liou, K. N.: On the correlated k-distribution method for radiative transfer in nonhomogeneous atmospheres, J. Atmos. Sci., 49, 2139–2156, 1992. 1042

**SCIAMACHY lunar occultation water vapor measurements**

F. Azam et al.

Title Page

| Abstract | Introduction |
| Conclusions | References |
| Tables | Figures |

◄ | ►

Back | Close

Full Screen / Esc

Printer-friendly Version

Interactive Discussion

Gottwald, M. and Bovensmann, H. (Eds.): Exploring the Changing Earth's Atmosphere, ISBN:978-90-481-9895-5, Springer Dordrecht Heidelberg London New York, doi:10.1007/978-90-481-9896-2, 2011. 1031

Gurlit, W., Zimmermann, R., Giesemann, C., Fernholz, T., Ebert, V., Wolfrum, J., Platt, U., and Burrows, J. P.: Lightweight diode laser spectrometer CHILD (Compact High-altitude In-situ Laser Diode) for balloonborne measurements of water vapor and methane, Appl. Optics, 44, 91–102, 2005. 1031

Harries, J. E., Russell, J. M. I., Tuck, A. F., Gordley, L. L., Purcell, P., Stone, K., Bevilacqua, R. M., M., G., Nedoluha, G., and Traub, W. A.: Validation of measurements of water vapor from the Halogen Occultation Experiment (HALOE), J. Geophys. Res., 101, 10205–10216, doi:10.1029/95JD02933, 1996. 1048

Hoogen, R., Rozanov, V. V., and Burrows, J. P.: Ozone profiles from GOME satellite data: Algorithm description and first validation, J. Geophys. Res., 104, 8263–8280, 1999. 1038

Kirk-Davidoff, D. B. and Lamarque, J.-F.: Maintenance of polar stratospheric clouds in a moist stratosphere, Clim. Past, 4, 69–78, doi:10.5194/cp-4-69-2008, 2008. 1032

Kirk-Davidoff, D. B., Hintsa, E. J., Anderson, J. G., and Keith, D. W.: The effect of climate change on ozone depletion through changes in stratospheric water vapour, Nature, 402, 399–401, 1999. 1032

Kley, D., Russell III, J. M., Phillips, C., and Eds.: SPARC assessment upper tropospheric and stratospheric water vapour, WCRP-No. 113, WMO/TD-No. 1043, SPARC Report No. 2, 2000. 1048

Kratz, D. P., Chou, M.-D., Yan, M. M.-H., and Ho, C.-H.: Minor trace gas radiative forcing calculations using the k distribution method with one-parameter scaling, J. Geophys. Res., 103, 31647–31656, doi:10.1029/1998JD200009, 1998. 1042

Lahoz, W. A., Carr, E. S., Froidevaux, L., Harwood, R. S., Kumer, J. B., Mergenthaler, J. L., Peckham, G. E., Read, W. G., Ricaud, P. D., Roche, A. E., and Waters, J. W.: Northern hemisphere mid – stratosphere vortex processes diagnosed from $H_2O$, $N_2O$, and potential vorticity, Geophys. Res. Lett., 20, 2671–2674, doi:10.1029/93GL02475, 1993. 1033

Lahoz, W. A., O'Neill, A., Heaps, A., Pope, V. D., Swinbank, R., Harwood, R. S., Froidevaux, L., Read, W. G., Waters, J. W., and Peckham, G. E.: Vortex dynamics and the evolution of water vapour in the stratosphere of the southern hemisphere, Q. J. Roy. Meteorol. Soc., 122, 423–450, doi:10.1002/qj.49712253007, 1996. 1033

**SCIAMACHY lunar occultation water vapor measurements**

F. Azam et al.

Title Page

Abstract | Introduction

Conclusions | References

Tables | Figures

|◄ | ►|

◄ | ►

Back | Close

Full Screen / Esc

Printer-friendly Version

Interactive Discussion

Lambert, A., Read, W. G., Livesey, N. J., Santee, M. L., Manney, G. L., Froidevaux, L., Wu, D. L., Schwartz, M. J., Pumphrey, H. C., Jimenez, C., Nedoluha, G. E., Cofield, R. E., Cuddy, D. T., Daffer, W. H., Drouin, B. J., Fuller, R. A., Jarnot, R. F., Knosp, B. W., Pickett, H. M., Perun, V. S., Snyder, W. V., Stek, P. C., Thurstans, R. P., Wagner, P. A., Waters, J. W., Jucks, K. W., Toon, G. C., Stachnik, R. A., Bernath, P. F., Boone, C. D., Walker, K. A., Urban, J., and Murtagh, D.: Validation of the Aura Microwave Limb Sounder middle atmosphere water vapor and nitrous oxide measurements, J. Geophys. Res., 112, 1–24, 2007. 1049

Li, J. and Barker, H. W.: A Radiation Algorithm with Correlated-k Distribution, Part I: Local Thermal Equilibrium., Physics, 62, 286–309, doi:10.1175/JAS-3396.1, 2004. 1042

Livesey, N. J., Synder, W. V., Read, W. G., and Wagner, P. A.: Retrieval algorithms for the EOS Microwave Limb Sounder (MLS), IEEE T. Geosci. Remote, 44, 1144–1155, 2006. 1049

Michelsen, H. A., Irion, F. W., Manney, G. L., Toon, G. C., and Gunson, M. R.: Features and trends in Atmospheric Trace Molecule Spectroscopy (ATMOS) version 3 stratospheric water vapor and methane measurements, J. Geophys. Res., 105, 22713–22724, doi:10.1029/2000JD900336, 2000. 1031

Pan, L. L., Randel, W. J., Massie, S. T., Kanzawa, H., Sasano, Y., Nakajima, H., Yokota, T., and Sugita, T.: Variability of polar stratospheric water vapor observed by ILAS, J. Geophys. Res., 107, 8214, doi:10.1029/2001JD001164, 2002. 1031

Pan, L. L., Bowman, K. P., Shapiro, M., Randel, W. J., Gao, R. S., Campos, T., Davis, C., Schauffler, S., Ridley, B. A., Wei, J. C., and Barnet, C.: Chemical behavior of the tropopause observed during the Stratosphere-Troposphere Analyses of Regional Transport experiment, J. Geophys. Res., 112–124, doi:10.1029/2007JD008645, 2007. 1031

Peter, T.: Microphysics and heterogeneous chemistry of polar stratospheric clouds, Annu. Rev. Phys. Chem., 48, 785–822, 1997. 1046

Rodgers, C. D.: Inverse Methods for Atmospheric Sounding: Theory and Practice, World Scientific, Singapore, 2000. 1034, 1045

Rothman, L., Gordon, I., Barbe, A., Benner, D. C., Bernath, P., Birk, M., Brown, L., Campargue, A., Champion, J.-P., Chance, K., Coudert, L., Dana, V., Devi, V., Fally, S., Flaud, J.-M., Gamache, R., Goldman, A., Jacquemart, D., Kleiner, I., Lacome, N., Lafferty, W., Mandin, J., Massie, S., Mikhailenko, S., Miller, C., Moazzen-Ahmadi, N., Naumenko, O., Nikitin, A., Orphal, J., Perevalov, V., Perrin, A., Predoi-Cross, A., Rinsland, C., Rotger, M., Simeckova, M., Smith, M., Sung, K., Tashkun, S., Tennyson, J., Toth, R., Vandaele, A., and Vander Auwera, J.: The HITRAN 2008 molecular spectroscopic database, J. Quant. Spectr. Radiative

Transfer, 110, 533–572, doi:10.1016/j.jqsrt.2009.02.01, Elsevier, 2009. 1038

Rozanov, A.: Modelling of the radiative transfer through a spherical planetary atmosphere: application to the atmospheric trace gas retrieval from occultation and limb measurements in UV-Vis-NIR, Ph.D. thesis, Universität Bremen, 2001. 1038

Rozanov, A., Rozanov, V., Buchwitz, M., Kokhanovsky, A., and Burrows, J. P.: SCIATRAN 2.0-A new radiative transfer model for geophysical applications in the 175–2400 nm spectral region, Adv. Space Res., 36, 1015–1019, doi:10.1016/S0273-1177(02)00095-9, 2005. 1038

Rozanov, A., Weigel, K., Bovensmann, H., Dhomse, S., Eichmann, K.-U., Kivi, R., Rozanov, V., Vömel, H., Weber, M., and Burrows, J. P.: Retrieval of water vapor vertical distributions in the upper troposphere and the lower stratosphere from SCIAMACHY limb measurements, Atmos. Meas. Tech., 4, 933–954, doi:10.5194/amt-4-933-2011, 2011. 1038

Rozanov, A. V., Rozanov, V. V., and Burrows, P. J.: Combined differential-integral approach for the radiation field computation in a spherical shell atmosphere: Nonlimb geometry, J. Geophys. Res., 105, 22937–22942, doi:10.1029/2000JD900378, 2000. 1038

Rozanov, V. V., Diebel, D., Spurr, R. J. D., and Burrows, J. P.: GOMETRAN: A radiative transfer model for the satellite project GOME, the plane-parallel version, J. Geophys. Res., 102, 16683–16695, doi:10.1029/96JD01535, 1997. 1038

Russell, J. M., I., Tuck, A. F., Gordley, L. L., Park, J. H., Drayson, S. R., Harries, J. E., Cicerone, R. J., and Crutzen, P. J.: HALOE Antarctic observations in the spring of 1991, Geophys. Res. Lett., 20, 719–722, doi:10.1029/93GL00497, 1993a. 1033

Russell, J. M. I., Gordley, L. L., Park, J. H., Drayson, S. R., Hesketh, W. D., Cicerone, R. J., Tuck, A. F., Frederick, J. E., Harries, J. E., and Crutzen, P. J.: The Halogen Occultation Experiment, J. Geophys. Res., 98, 10777–10797, doi:10.1029/93JD00799, 1993b. 1047

Schoeberl, M., Douglass, A., Hilsenrath, E., Bhartia, P., Beer, R., Waters, J., Gunson, M., Froidevaux, L., Gille, J., Barnett, J., Levelt, P., and DeCola, P.: Overview of the EOS aura mission, Geoscience and Remote Sensing, 44, 1066–1074, doi:10.1109/TGRS.2005.861950, 2006. 1048

Solomon, S., Rosenlof, K. H., Portmann, R. W., Daniel, S. M. D., Sanford, T. J., and Plattner, G. K.: Contributions of Stratospheric Water Vapor to Decadal Changes in the Rate of Global Warming, Science, 327, 1219–1223, doi:10.1126/science.1182488, 2010. 1031

Stiller, G. P., Kiefer, M., Eckert, E., von Clarmann, T., Kellmann, S., García-Comas, M., Funke, B., Leblanc, T., Fetzer, E., Froidevaux, L., Gomez, M., Hall, E., Hurst, D., Jordan, A., Kämpfer, N., Lambert, A., McDermid, I. S., McGee, T., Miloshevich, L., Nedoluha, G., Read, W.,

**SCIAMACHY lunar occultation water vapor measurements**

F. Azam et al.

Title Page

Abstract | Introduction

Conclusions | References

Tables | Figures

|◄ | ►|

◄ | ►

Back | Close

Full Screen / Esc

Printer-friendly Version

Interactive Discussion

Schneider, M., Schwartz, M., Straub, C., Toon, G., Twigg, L. W., Walker, K., and Whiteman, D. N.: Validation of MIPAS IMK/IAA temperature, water vapor, and ozone profiles with MOHAVE-2009 campaign measurements, Atmos. Meas. Tech. Discuss., 4, 4403–4472, doi:10.5194/amtd-4-4403-2011, 2011. 1049

Tikhonov, A. N.: On the solution of incorrectly stated problems and a method of regularization, 151, Dokl. Acad. N., 1963. 1036

Tikhonov, A. N. and Arsenin, V. Y. .: Solutions of ill-Posed Problems, Wiley, New York, 1977. 1036

von Clarmann, T., Höpfner, M., Kellmann, S., Linden, A., Chauhan, S., Funke, B., Grabowski, U., Glatthor, N., Kiefer, M., Schieferdecker, T., Stiller, G. P., and Versick, S.: Retrieval of temperature, $H_2O$, $O_3$, $HNO_3$, $CH_4$, $N_2O$, $ClONO_2$ and ClO from MIPAS reduced resolution nominal mode limb emission measurements, Atmos. Meas. Tech., 2, 159–175, doi:10.5194/amt-2-159-2009, 2009. 1049

von Savigny, C., Ulasi, E. P., Eichmann, K.-U., Bovensmann, H., and Burrows, J. P.: Detection and mapping of polar stratospheric clouds using limb scattering observations, Atmos. Chem. Phys, 5, 3071–3079, doi:10.5194/acp-5-3071-2005, 2005. 1046

Waters, J. W., Froidevaux, L., Harwood, R. S., Jarnot, R. F., Pickett, H. M., Read, W. G., Siegel, P. H., Coeld, R. E., Filipiak, M. J., Flower, D. A., Holden, J. R., Lau, G. K., Livesey, N. J., Manney, G. L., Pumphrey, H. C., Santee, M. L., Wu, D. L., Cuddy, D. T., Lay, R. R., Loo, M. S., Perun, V. S., Schwartz, M. J., Stek, P. C., Thurstans, R. P., Boyles, M. A., Chandra, K. M., Chavez, M. C., Chen, G. S., Chudasama, M. V., Dodge, R., Fuller, R. A., Girard, M. A., Jiang, . J. J., Jiang, Y., Knosp, B. W., LaBelle, R. C., Lam, J. C., Lee, K. A., Miller, D., Oswlad, J. E., Patel, N. C., Pukala, D. M., Quintero, O., Sca, D. M., Van Synder, W., Tope, M. C., Wagner, P. A., and Walch, M. J.: The Earth Observing System Microwave Limb Sounder (EOS MLS) on the Aura satellite, IEEE T. Geosci. Remote, 44, 1075–1092, 2006. 1048, 1049

Wiscombe, W. J. and Evans, J. W.: Exponential-sum fitting of raditaitve transmission functions, J. Comput. Phys., 24, 416–444, 1977. 1041

**SCIAMACHY lunar occultation water vapor measurements**

F. Azam et al.

Title Page

| Abstract | Introduction |
| Conclusions | References |
| Tables | Figures |

|◄ | ►|

◄ | ►

Back | Close

Full Screen / Esc

Printer-friendly Version

Interactive Discussion

**Table 1.** Pressure, Temperature and Coefficients Database Grids: ESFT retrieval was performed using different pressure, temperature and coefficients grids.

| Pressure | Temperature | Coefficients |
|---|---|---|
| 10 | 9 | 10 |
| 32 | 9 | 10 |
| * 32 | 9 | 10 |
| 32 | 22 | 10 |
| 32 | 22 | 15 |

* The third row indicates the same grid as in the second row but with different distribution of pressures and temperatures.

Title Page

Abstract    Introduction

Conclusions    References

Tables    Figures

|◄    ►|

◄    ►

Back    Close

Full Screen / Esc

Printer-friendly Version

Interactive Discussion
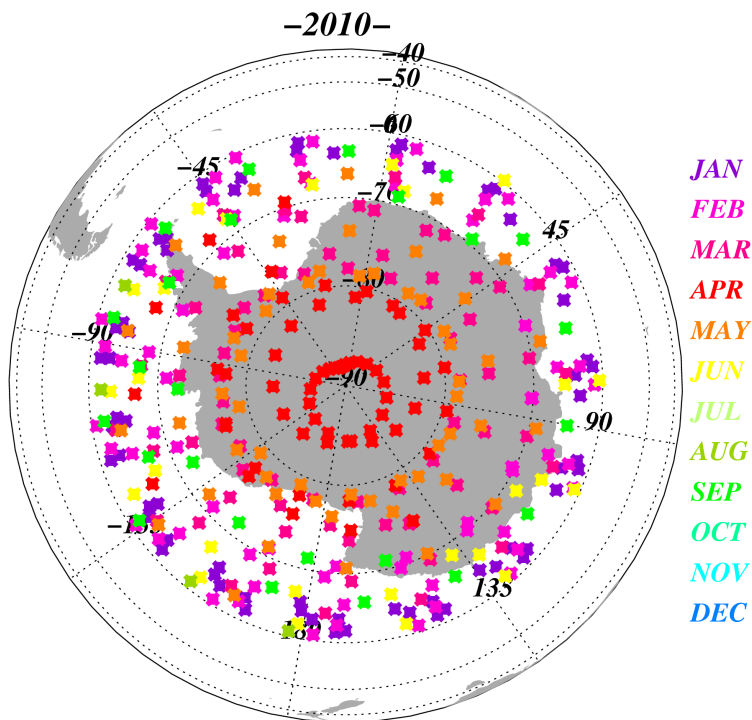
**Fig. 1.** SCIAMACHY lunar occultation tangent points in 2010; the latitudes vary within 59° S–89° S.

Title Page

Abstract | Introduction

Conclusions | References

Tables | Figures

|◄ | ►|

◄ | ►

Back | Close

Full Screen / Esc

Printer-friendly Version

Interactive Discussion
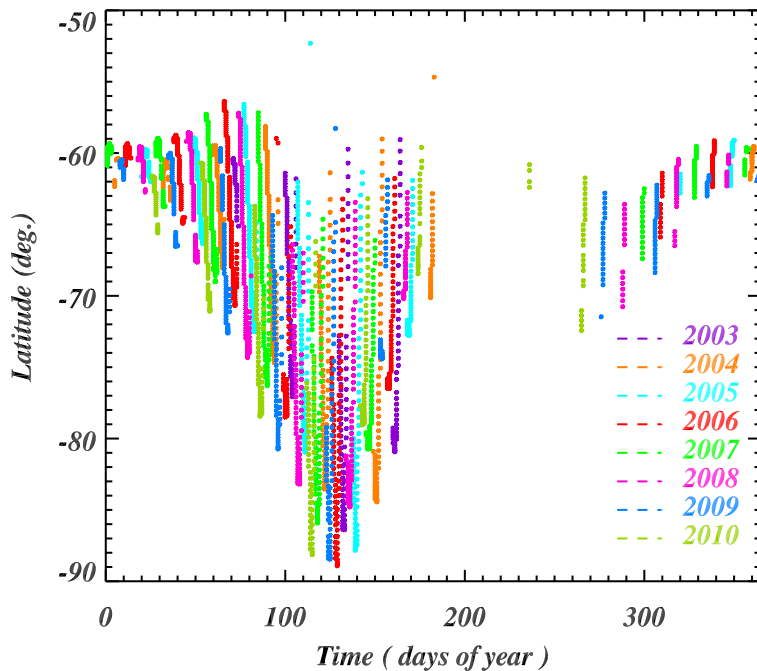
**Fig. 2.** SCIAMACHY lunar occultation latitudinal distribution for the years 2003–2010; each year the latitudes vary considerably between 59° S–89° S.
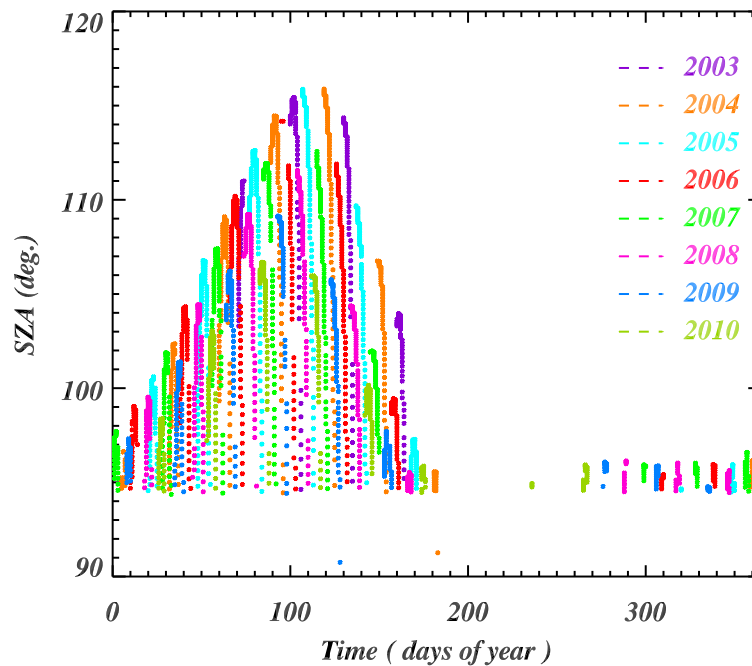
**Fig. 3.** SCIAMACHY lunar occultation SZA distribution for the years 2003–2010; each year the SZA span is within 94° and 115°.
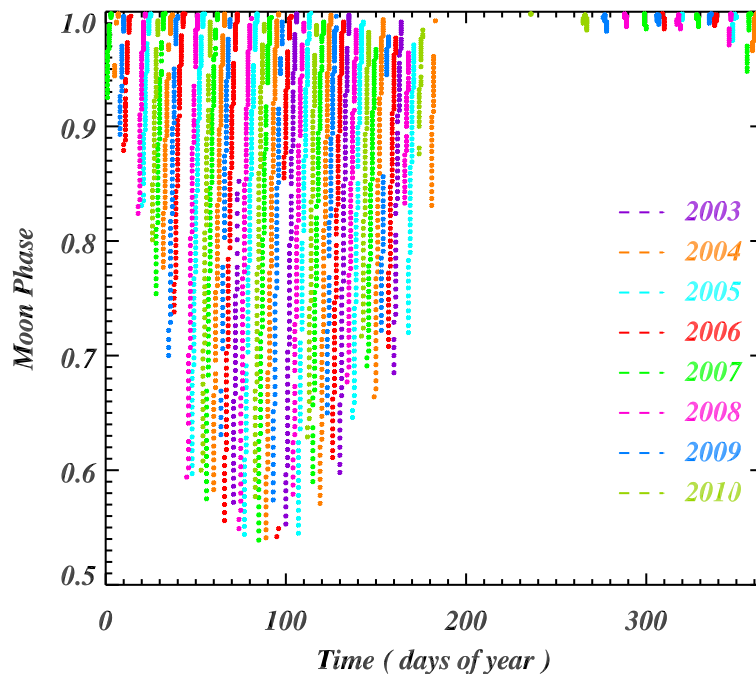
Full Screen / Esc

**Fig. 4.** SCIAMACHY lunar occultation moon phase distribution for the years 2003–2010; the observed moon phase values vary around 0.5–0.99.
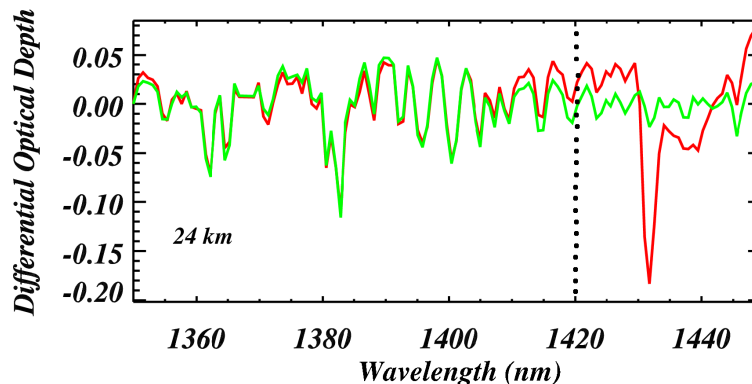
**Fig. 5.** Spectral plot for the wavelength window 1350–1450 nm and 24 km tangent height: red line is the measured water vapor differential absorption spectrum. Green line is the corresponding modelled differential optical depth. A strong $CO_2$ absorption line is present around 1430 nm. Wavelength section 1350–1420 nm was selected for the retrieval. (Measurement: 13 March 2006, orbit = 21 085, sza = 109.137, moon phase = 0.93).
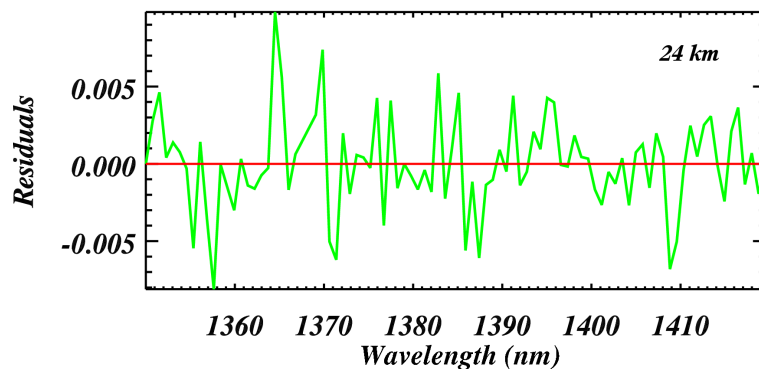
**Fig. 6.** Residual plot for the selected wavelength window 1350–1420 nm (corresponds to the same measurement as for Fig. 5): the residuals signify the difference between the measured and the simulated differential transmitted spectra. The residuals are about 0.5 %.
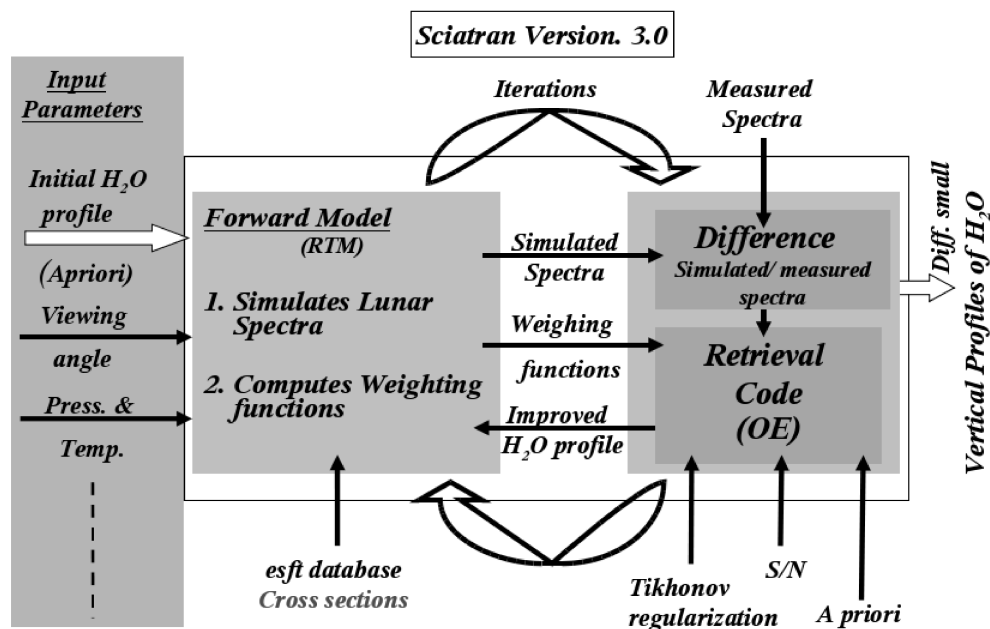
**Fig. 7.** SCIATRAN: Setup for the retrieval by ESFT method. The functioning of forward model and the retrieval parts are elaborated here.
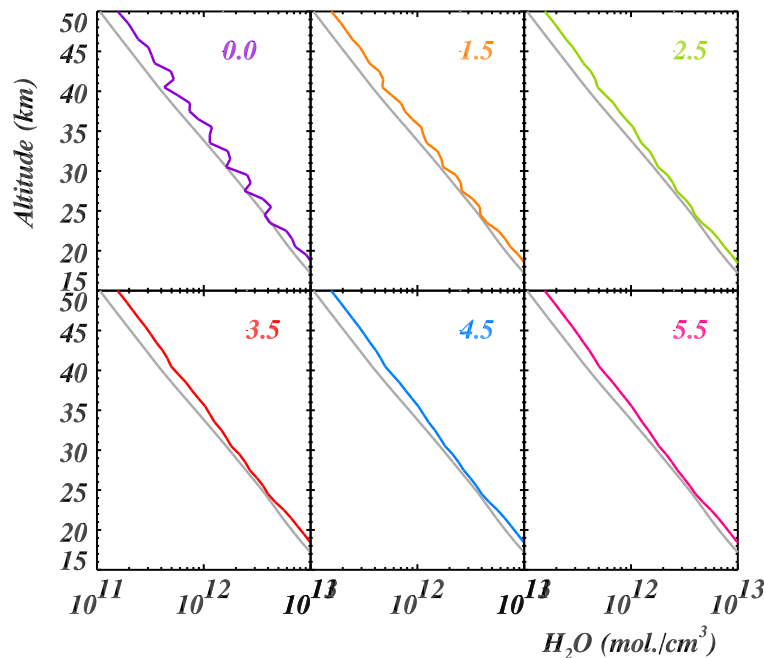
**Fig. 8.** Number density profiles with different Tikhonov parameters: Tihkonov parameter 3.5 was selected for the retrieval (Measurement: 13 March 2006, orbit = 21 085, sza = 109.137, moon phase = 0.93).
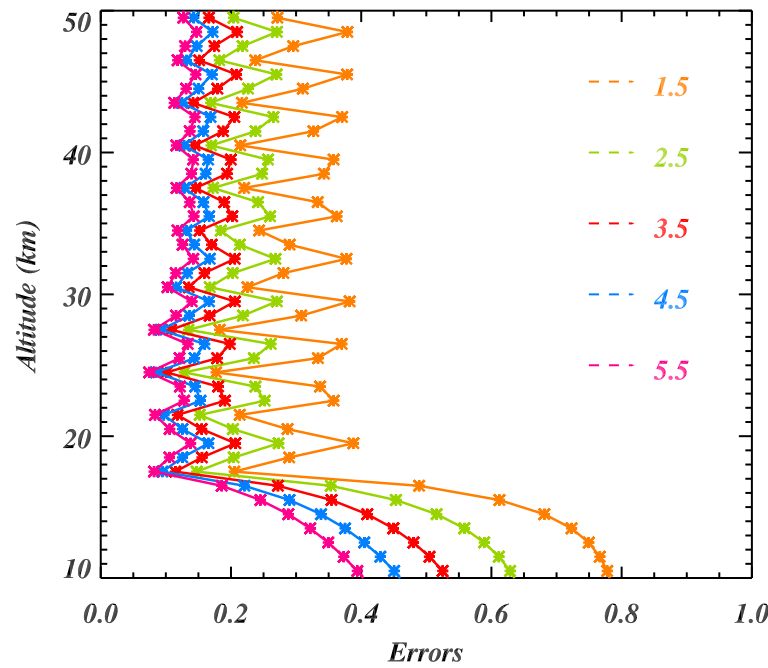
**Fig. 9.** Theoretical error profiles corresponding to the profiles in Fig. 8 (except for 0.0): errors are within a reasonable range for the selected Tikhonov value of 3.5.

F. Azam et al.
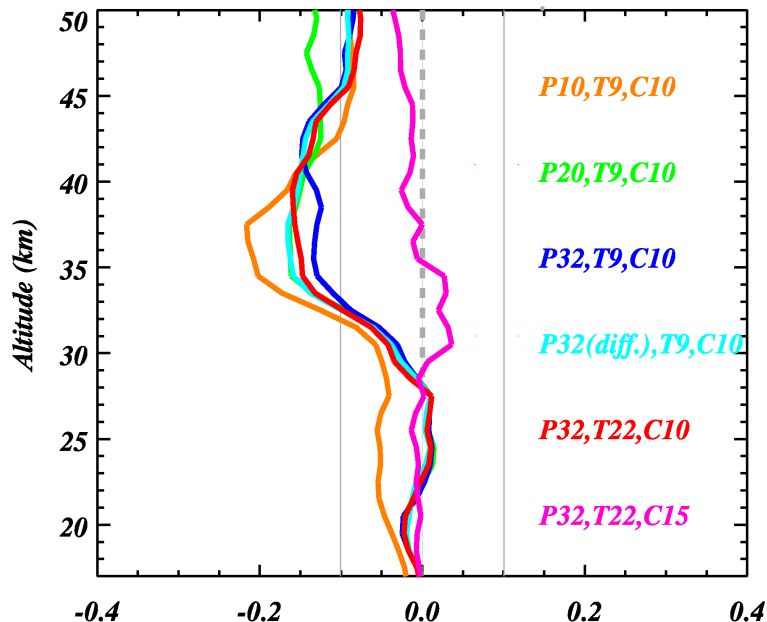
**Fig. 10.** The LBL-ESFT comparison for the year 2008: ESFT retrieval performed at different grids with different pressure, temperature, and number of coefficients and compared with LBL. The results are shown as the relative differences i.e. (LBL-ESFT)/LBL.
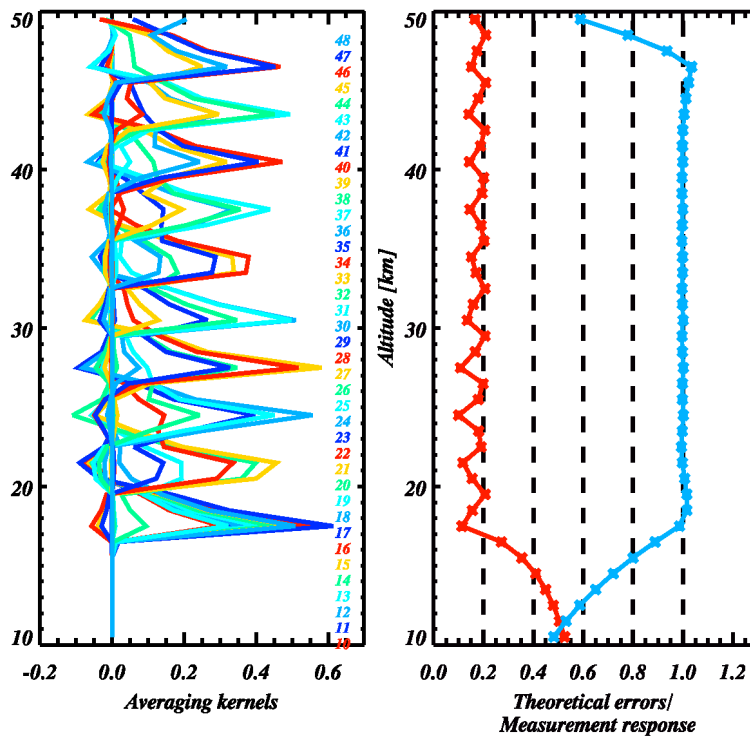
**Fig. 11.** The left panel shows the averaging kernels and the right panel shows the theoretical errors (red line) and the measurement response function (blue line). The measurement is on 13 March 2006, orbit = 21 085, sza = 109.137, moon phase = 0.93.
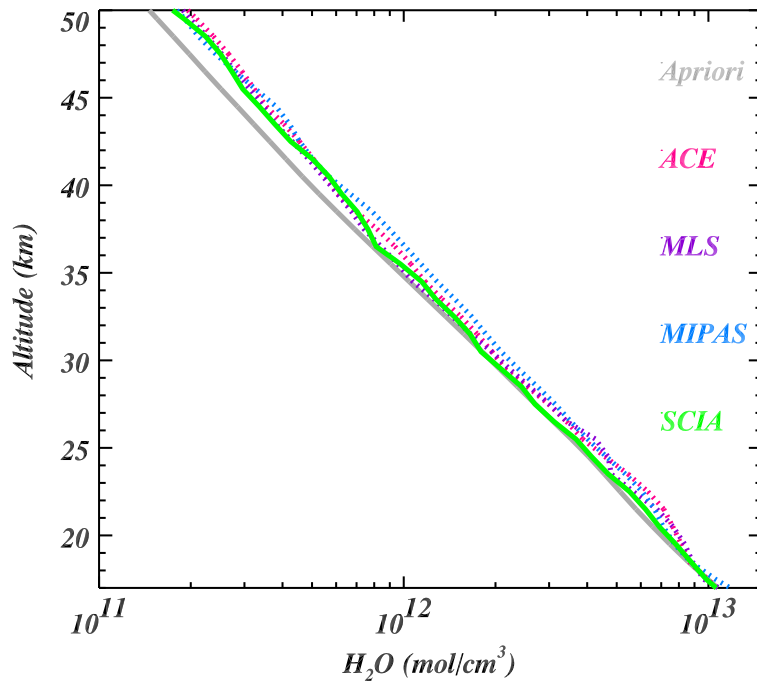
**Fig. 12.** An example of the retrieved SCIAMACHY lunar occultation water vapor profile from 10 January 2009, orbit number 35889. For this measurement three collocations are found with ACE-FTS(ss29145), MLS(T505691134), MIPAS(35894).

Title Page

Abstract | Introduction

Conclusions | References

Tables | Figures

|◄ | ►|

◄ | ►

Back | Close

Full Screen / Esc

Printer-friendly Version

Interactive Discussion

**Fig. 13.** SCIAMACHY-ACE comparison statistics for the period 2004–2009 based on 302 collocations with combined ACE-FTS sunrise and sunset events.
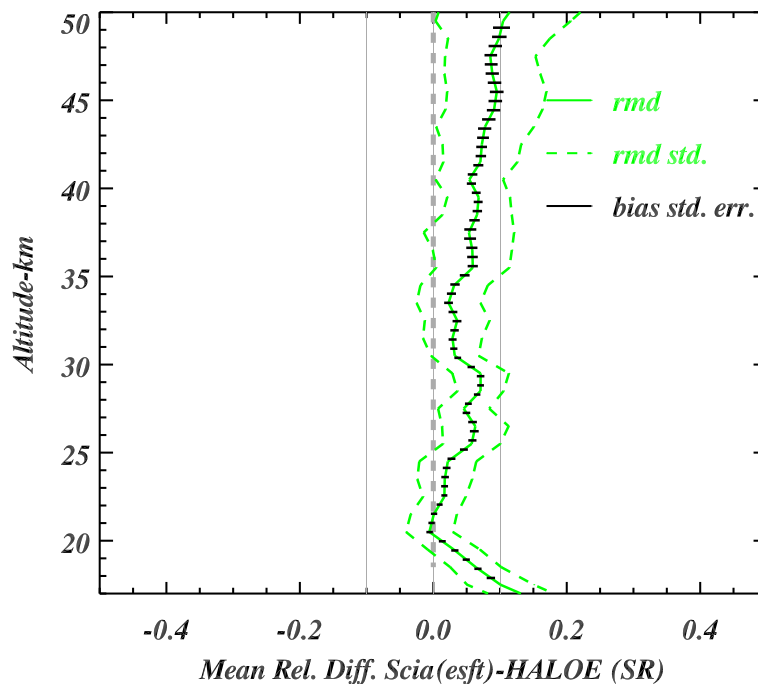
**Fig. 14.** SCIAMACHY-HALOE comparison statistics for the period 2003–2005 based on 52 collocations with HALOE sunrise events where none was found with sunset.
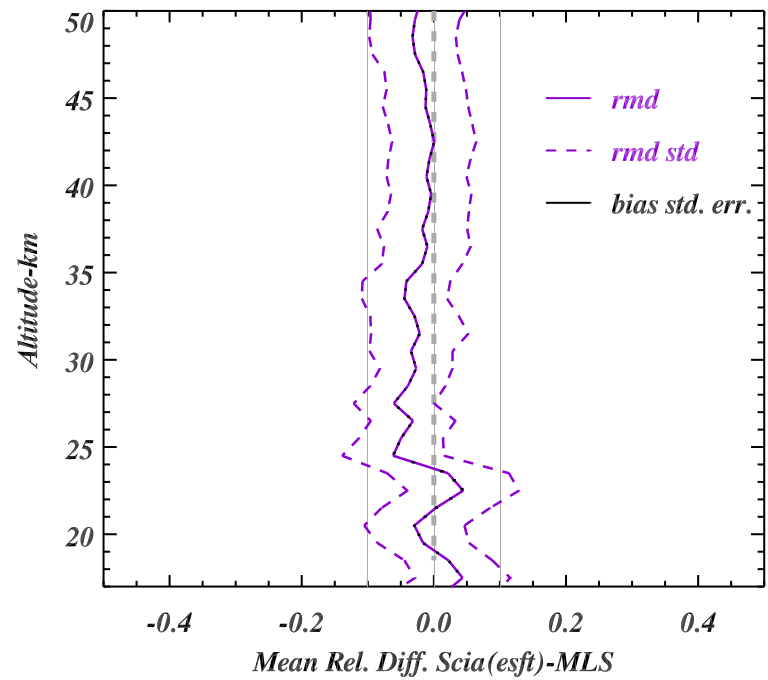
**Fig. 15.** SCIAMACHY-MLS comparison statistics for the period 2004–2010 based on 1321 collocations.
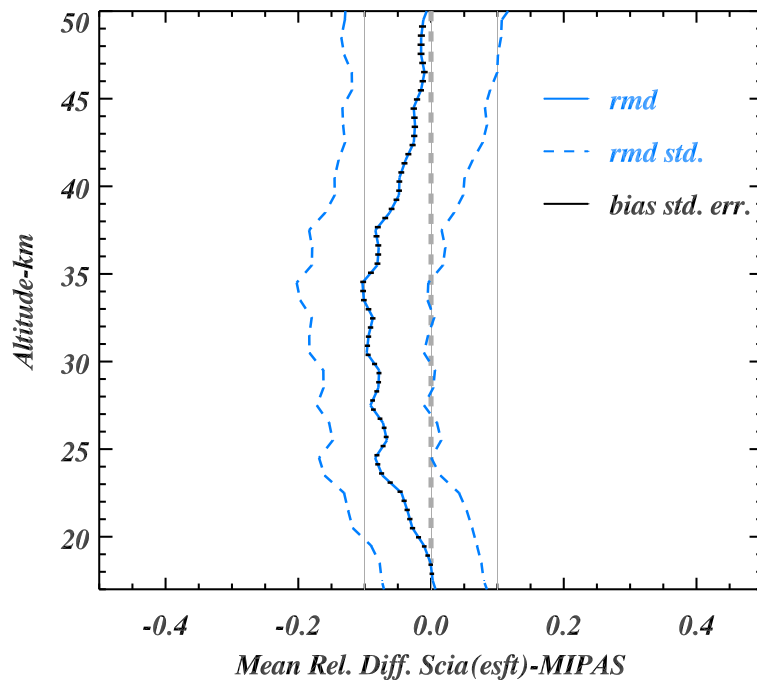
**Fig. 16.** SCIAMACHY-MIPAS comparison statistics for the period 2005–2010 based on 489 collocations.